Available online at www.sciencedirect.com
SCIENCE DIRECT®
Journal of the European Ceramic Society 25 (2005) 2175–2180
www.elsevier.com/locate/jeurceramsoc

Nanocrystalline anatase thin films prepared from redispersible sol–gel powders

R.C. Kaminski [a], S.H. Pulcinelli [a], A.F. Craievich [b], C.V. Santilli [a,*]

[a] *UNESP, Instituto de Quimica, P.O. Box 355, 14800-900 Araraquara, SP, Brazil*
[b] *Instituto de Física, USP, São Paulo, SP, Brasil*

Available online 12 April 2005

Abstract

Transparent thin films of nanocrystalline anatase were obtained by dip-coating process using an ethanolic suspension of redispersed nanoparticles. This suspension was prepared by sol–gel route and their redispersability achieved by surface grafting of *para*-toluene–sulfonic acid and acetylacetone. The effects of the acetylacetone content on the powder redispersibility and on the structural evolution of films were determined by small angle X-ray scattering, X-ray reflectometry and X-ray diffraction for different firing temperatures. The results demonstrated that the porous structure of the studied films consist of agglomerates of primary particles with two levels of porosity. The control of the amount of capping ligand allows for a fine-tuning of the average pore size of the dried films. Upon increasing the firing temperature up to 500 °C, progressive increase in apparent density, average pore size of films and average crystallite size of powders were observed.

Keywords: Films; Sol–gel processing; Sintering; Porosity; TiO_2

1. Introduction

Nanocrystalline titania-based films have attracted great scientific and technological interest because of their interesting electrical, optical and catalytic properties, and because of several potential applications as a basic material for varistors,[1] capacitors,[1] gas and humidity sensors,[2] and photovoltaic devices.[3] The surface properties are of paramount importance for nanosized grained materials, for which the surface to volume ratio is much greater than in bulk solids, making the former particularly appealing for the development of gas sensors and photovoltaic applications.[2,3] Many chemical methods have been considered so far as candidates for preparation of uniform amorphous TiO_2 films, being the sol–gel route the most practical for controlling the features of the nanoscopic structure.[2–7] The most frequently used precursors for titania films through sol–gel processing are sols obtained by hydrolysing acetic acid or acetilacetone complexed titanium alkoxides.[6,7] However, even if the resulting nanoparticles are monodispersed in size, they tend to aggregate so as minimizing the surface free energy. Because of surface reactivity, the particle-to-particle interaction is strong and thus agglomeration becomes irreversible, especially after drying. Furthermore, the condensation of the surface hydroxyl groups pulls together the constituent particles of the sol into a compact mass and, thus, the final particles grow up to a size much larger than that of the initial one.[7]

The improvement of the kinetic stability of sols and the development of redispersible nanoparticles is of paramount importance for the industrial use of the sol–gel process in the fabrication of ceramic films with fine-scaled microstructure. The most frequently used approach to prevent the agglomeration and growth of nanoparticles is the substitution of the surface hydroxyl groups by another functional group, like organic complexing molecules, that do not condense as OH does and that could eventually provide the redispersibility of the powdered xerogel.[6,7] Nevertheless, subsequent heat treatments—that should be carried out in order to remove the organic groups—may strongly affect the regular nanostructure of the freshly derived film.

* Corresponding author. Tel.: +55 16 33016645; fax: +55 16 33227932.
E-mail address: santilli@iq.unesp.br (C.V. Santilli).

0955-2219/$ – see front matter © 2005 Elsevier Ltd. All rights reserved.
doi:10.1016/j.jeurceramsoc.2005.03.026

In this paper, the influence of both the firing temperature and the amount of complexing ligand on the nanostructural features of anatase transparent thin films was investigated. The films were deposited by dip-coating using an ethanolic suspension of redispersed nanoparticles prepared by sol–gel route, whose redispersibility was achieved by controlled modification of the surface with acetylacetone (Acac) and *para*-toluene–sulfonic acid (PTSH). [6]

2. Experimental

The preparation of redispersible anatase nanoparticles was based on the sol–gel route proposed by Scolan and Sanchez.[6] To a solution of acetylacetone (the acetylacetonate ligand bonded to titanium will be noted as Acac) in isopropanol, titanium tetraisopropoxide ($Ti(OProp^i)_4$) was added slowly and the mixture was stirred at room temperature for 15 min. Hydrolysis of the clear mixture was performed by drop-wise addition of PTSH aqueous solution. The acidified solution (pH 2.3) was refluxed for 18 h at 60 °C under magnetic stirring. The flask was fitted with a condenser and a $CaCl_2$ trap to avoid moisture exposure. The nominal complexing ratio, defined as C = [Acac]/[Ti] was varied between 0 and 4. The hydrolysis ratio, H = $[H_2O]$/[Ti], and the acidity ratio, A = [PTSH]/[Ti] were fixed at 4 and 0.2, respectively. The redispersible powders were obtained after solvent evaporation at 100 °C for 24 h.

Transparent thin films of nanocrystalline anatase were deposited on clean Corning boron–silicate glass substrates by dip-coating process using an ethanolic suspension containing 4 wt.% of redispersed nanoparticles. Every deposition involved 1 dip at a withdrawal speed of 8 cm/min. For the films studied by small-angle X-ray scattering (SAXS), 10 successive layers were deposited on 0.05 mm thick mica sheets to obtain thick enough samples (≈100 nm). After each dipping, the samples were dried at 100 °C and then subjected to slow heating at a rate of 5 °C/min to a desired temperature from 300 to 500 °C and then held at that for 1 h. This heating protocol was applied also to the thermal treatment of dried powders.

Simultaneous thermogravimetric (TG) and differential thermoanalysis (DTA) of dried powders were performed, from room temperature up to 800 °C under oxygen flux, by using a SDT2960 (TA Instruments) apparatus at a heating rate of 10 °C/min. The crystalline phases present in dried and fired powders were analyzed by X-ray powder diffraction (XRPD) with a Siemens D5000 diffractometer (Cu Kα radiation, λ = 1.541 Å) with a curved graphite monochromator, and a fix divergence slit of 1/8° in a Bragg–Brentano configuration. Intensity data were collected by the step counting method (step 0.02° and time 3 s) in a 2θ range between 10 and 80°. This equipment was also used to measure the X-ray reflectivity (XRR) of the films, which yields their thickness and apparent density. The accuracy for density and thickness determinations is about 7% and 0.5 nm, respectively.

The SAXS study of redispersed sols and of coated films was performed using the synchrotron SAXS beam line of LNLS (Campinas, Brazil). This beam line is equipped with an asymmetrically cut and bent silicon (1 1 1) monochromator that yields a monochromatic (λ = 1.608 Å) and horizontally focused beam. An ionisation chamber, placed downstream from the sample was used to monitor the intensity of the incident beam and to determine the sample transmission. A vertical position-sensitive X-Ray detector located at 776 mm from the sample and a multichannel analyser were used to record the scattering intensity, $I(q)$, as a function of the modulus of scattering vector $q = (4\pi/\lambda)\sin(\varepsilon/2)$, ε being the scattering angle. The parasitic scattering intensity produced by the solvent, substrate and air was subtracted from the total scattering intensity. The resulting curves were normalized to account for the effects related to natural decay in the intensity of the synchrotron source, detector sensitivity and sample transmission.

3. Results and discussion

Fig. 1 shows the relative mass loss (TG) and differential thermal analysis (DTA) curves corresponding to the dried powders prepared with different complexing ratio. The endothermic mass loss (4–6 wt.%) observed for temperatures lower than 110 °C can be attributed to water and organics desorption. A release (8–10 wt.%) and combustion (weak exothermic peak) of weakly bonded or adsorbed organic species is verified between 180 and 220 °C. A significant mass loss accompanied by an intense exothermic peak corresponding to the removal of organics is apparent between 310 and 460 °C. The mass loss involved in this process increases from 24 to 52 wt.% by the increase of [Acac]/[Ti] ratio from 0 to 4. The oxidation of the organics content of complexing species usually takes place within this temperature range, as indicated by the strong complexing linkage between titanium atoms and organics. The presence of the complexed form of Acac and PTSH was confirmed by ^{13}C and ^{1}H NMR spectra of dried powders.

Fig. 2 compares the XRPD patterns of powders with different complexing ligand ratios treated at different temperatures. The dried powder prepared without Acac is amorphous and cannot be redispersed, while the patterns of powders containing Acac complexing ligand present a broad (1 0 1) peak, characteristic of nanocrystalline anatase. Heat treatments up to 300 °C do not lead to remarkable changes in XRPD patterns. When the firing temperature increases up to 400 °C, the maximum intensity of the Bragg peaks increases, while their width decreases, thus evidencing the growth of the crystallites. The average size of the anatase crystallites was calculated from the measured width of the [1 0 1] Bragg peak using the Scherrer relation and assuming that the peak broadening is essentially due to size effects. The average sizes of the anatase crystallites, within accuracy of 15%, are reported in Table 1.

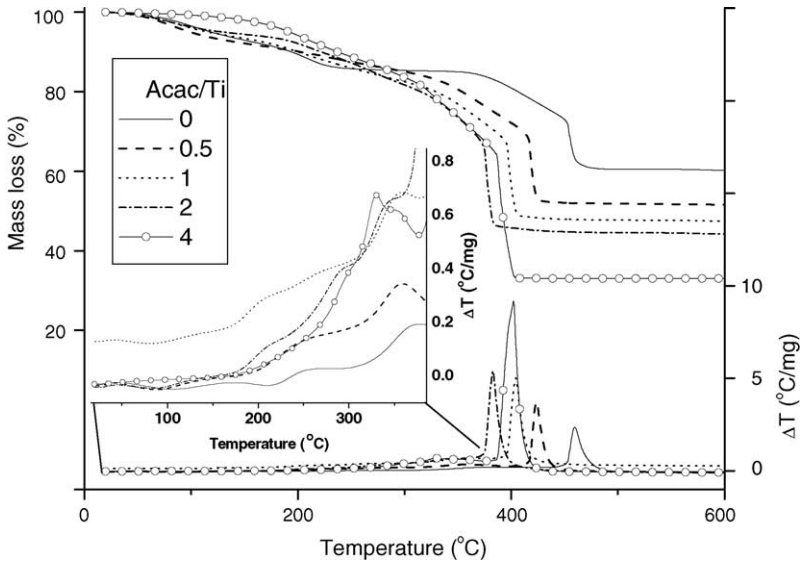

Fig. 1. Thermogravimetric and DTA curves of powders prepared with different complexing ratio C = [Acac]/[Ti]. The inset shows a magnification of DTA curves for temperatures lower than 400 °C.

The experimental XRR curves were collected for all the studied films fired at different temperatures, but, for clarity, only the curves corresponding to those prepared with $C = 0.5$, 2 and 4 are displayed in Fig. 3. An increase in the critical angle for total reflection is observed for increasing temperatures in all cases, demonstrating that the higher the firing temperature the denser the films. This densification favours the films shrinkage and, consequently, the thickness reduction, as shown by the decrease in the period of the interference fringes of reflectivity curves. Furthermore, the appearance of interference fringes indicates that the films are continuous and present a nearly homogeneous thickness at nanometric level over large lateral dimensions. Experimental XRR curves were simulated using the theoretical procedure proposed by Nevot and Croce.[8] This fitting procedure yielded the following parameters: (i) the apparent density of the coating layer,

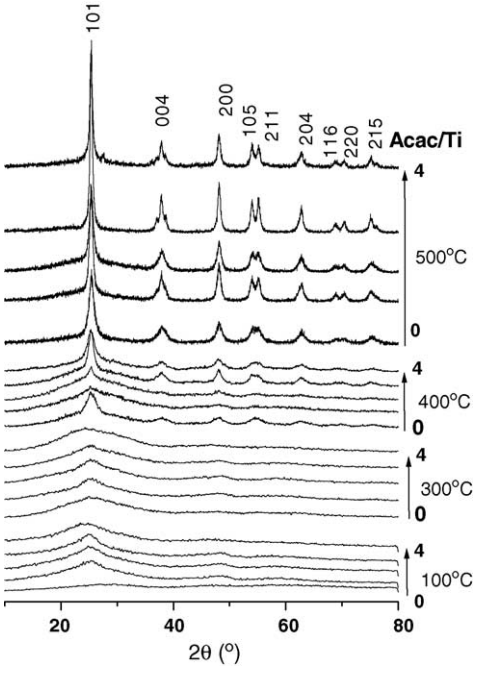

Fig. 2. XRPD patterns of powders prepared with different complexing ratio C = [Acac]/[Ti]. The patterns of samples treated at different temperatures were vertically translated for clarity.

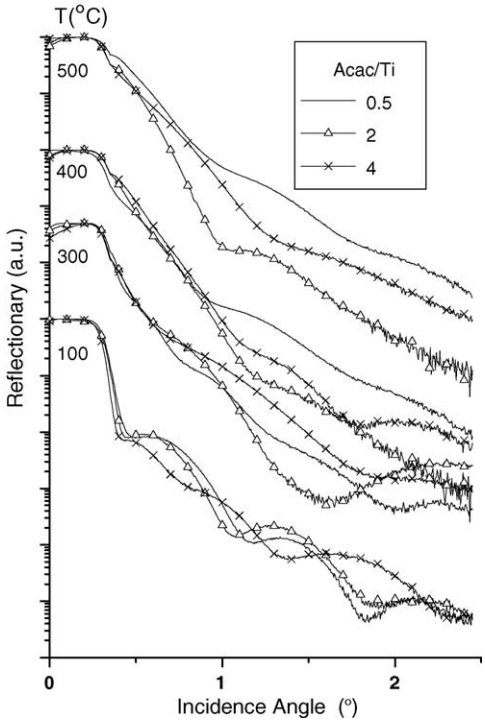

Fig. 3. X-ray reflectivity curves of films, treated at different temperatures, prepared from redispersed sol with different complexing ratio C = [Acac]/[Ti]. The curves were vertically translated for clarity.

Table 1
Structural parameters of sol, powders and films obtained from XRPD, XRR and SAXS measurements

	Crystallite size of powders (nm)	Density ($g.cm^{-3}$)	Thickness (nm)	Gyration Radius R_g (nm)	Packing factor, k	Correlation length, d (nm)
Acac/Ti T (°C)	0/ 0.5/ 1/ 2/ 4	0.5/ 1/ 2/ 4	0.5/ 1/ 2/ 4	0.5/ 1/ 2/ 4	0.5/ 1/ 2/ 4	0.5/ 1/2/ 4
sol	-/ -/ -/ -/-	-/ -/ -/	-/ -/ -/ -	-/ 0.9/ -/ 0.7	-/ 3.4/ - / 2.8	-/ 2.5/ -/2.0
100	-/0.9/0.9/1.2/0.9	2.6/ 2.0/ 2.7/ 2.4	13/ 11/ 9/ 12	0.4/ 0.5/ 0.4/ 0.6	0.1/1.0/0.6/ 0.0	1.9/ 1.6/1.9/ -
300	0.8/0.8/0.8/0.8/0.8	2.8/ 2.6/ 3.3/ 3.6	13/ 9/ 7/ 8	0.8/ 0.7/ 0.7/ 0.6	1.1/2.5/2.5/ 0.0	2.1/ 2.2/2.5/ -
400	1.8/4.0/0.8/0.9/2.1	3.1/ 3.4/ 3.8/ 3.8	10/ 7/ 7/ 7	-/ -/ -/ -	-/ -/- / -	-/ -/ -/ -
500	9.5/ 15/ 9.0/ 24/27	3.8/ 3.4/ 3.8/ 3.8	10/ 6/ 7/ 7	3.4/ 2.8/ 2.8/ 3.1	2.1/2.5/2.0/ 0.7	11/ 9.8/9.3/7.0

deduced from the critical angle, θ_c, for total reflection taking account for the elemental composition of films (the contribution from organics in the atoms proportion was evaluated from TG results, Fig. 1); and (ii) the thickness of the coating film deduced from the period of the oscillations in the reflectivity curves. The values of the density and thickness assuming a single film layer are also reported in Table 1.

SAXS curves corresponding to films prepared from powders with different complexing ratio and submitted to different firing temperatures are plotted in Fig. 4. The curve of the sol prepared with 15 wt.% of redispersed powder is also displayed. The SAXS patterns of sol and films treated at 500 °C present a well-defined peak, similar to that observed in previous studies of concentrated SnO_2 sols and SnO_2 films.[9] This peak was attributed to interference effects in the X-ray scattering amplitude coming from spatial correlation of particles in suspension and pores in the films. The intensity of this peak decreases for decreasing firing temperatures, being note clearly apparent in dried films. In the low q region, the intensity increases for decreasing q, indicating the presence of a coarser structural level. The scattering intensity produced by this type of structure formed by multiple (n) structural levels can be described by a semi-empirical equation proposed by Beaucage et al.[10] that obeys both Guinier and Porod asymptotic trends and takes into account the correlation effects:

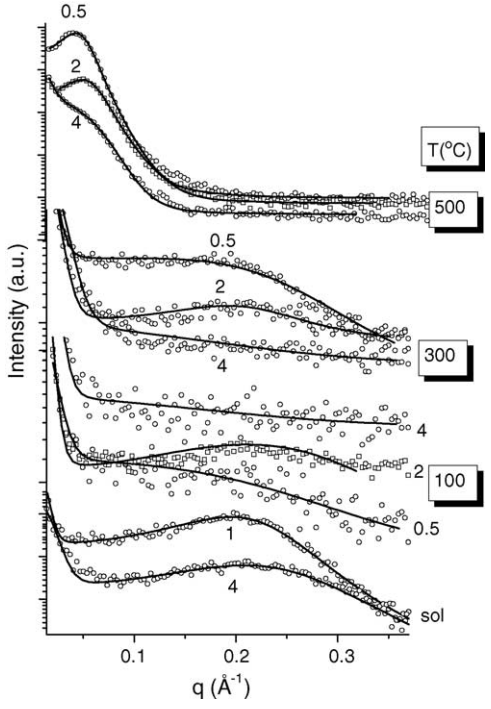

Fig. 4. SAXS curves for redispersed sols and films treated at different temperatures, prepared from sol with different complexing ratio C = [Acac]/[Ti]. The curves were vertically translated for clarity.

$$I(q) = \sum_{i=1}^{n} G_i e^{\frac{-q^2 R_{gi}^2}{3}} + B_i e^{\frac{-q^2 R_{g(i-1)}^2}{3}} \times \left[\frac{\left[\mathrm{erf}(qR_{gi}/\sqrt{6})\right]^3}{q} \right]^{P_i} S_i(q) \quad (1)$$

where R_g is the radius of gyration of scattering objects and the parameters G, B and P depend on the electron density contrast, size and shape of the objects, respectively. The structure function $S(q)$ for spherical nano-objects, in which the only correlation is a hard sphere interaction is given by:

$$S(q) = \frac{1}{1 + k\theta} \quad (2)$$

$k = 8V/V_0$, being the packing factor, where V is the average "hard-core" volume and V_0 is the average available volume to each sphere. The θ factor depends on the average inter-sphere distance d as follows: $\theta = 3[\sin(qd) - qd\cos(qd)]/(qd)^3$.

The fits of Eq. (1) to the experimental curves were performed by taking account both coarse ($n = 1$, $S_1(q) = 1$) and fine ($n = 2$, $S_2(q)$ given by Eq. (2)) structural levels. Although the crystal structure of anatase could give rise to anisotropic growth during firing, a satisfactory fit of Eq. (1), which holds for spherical shape, was obtained as displayed by continuous lines in Fig. 4. Despite the fact that the intensity produced by

the coarse level is described by Eq. (1), the absence of a trend towards a constant value for decreasing q (characteristic of a Gaussian function) hinders the accurate determination of R_{g1}. The low q region of SAXS curves was in all cases well fitted assuming $R_{g1} \approx 100$ nm, which corresponds to a rough characteristic size of the coarse structure. Thus, only the parameters related to the fine structure were precisely determined by the mentioned non-linear least square fitting procedure. The values of the relevant structural parameters (R_{g2}, k, and d) corresponding to the fine structure level are also reported in Table 1.

In the light of data listed in Table 1, the effect of the complexing ratio on the nanostructural feature of nanocrystalline anatase films can be explained as follows. Firstly, it is important to note that the average crystallite size in dried powders are close to the values of R_{g2} of fine particles in suspension, determined by SAXS. It indicates that each primary particle is formed by more than one crystallite. Furthermore, the scattering observed at low q region of SAXS curves indicates the presence of coarse objects ($R_{g1} > 100$ nm) attributed to the aggregates of primary particles. As the aggregation level in colloidal systems decreases by dilution, this assignment could be confirmed by SAXS measurements carried out as a function of the powder content in the suspension (data not shown). The relative contribution of the low q scattering with respect to the peak intensity at high q range decreases by dilution of suspension, and are not observed for solid contents lower than 4 vol.%, like that used for film deposition. Therefore, we infer that the fine and the coarse objects observed in SAXS curves of films are related to hierarchical structure resulting from the aggregation process induced by solvent evaporation during dip-coating. The values of R_{g2} in dried films are systematically smaller than that of the sol, and for samples fired at 500 °C R_{g2} is much lower than the average crystallite size. These findings suggest that the fine object probed by SAXS is in fact voids between primary particles.

The ill-defined maximum observed both for dried films and after firing at 300 °C can be explained by the weak degree of correlation revealed by the low value of the packing factor k, and also by the low electronic density contrast between the not empty pores and the anatase matrix. The later contribution is supported by the observed increase of k at increasing temperature from 110 to 300 °C without a remarkable increase of the amplitude of correlation peaks. Therefore, this result suggests that for dried films pores are at least partially filled with organics and the firing at 300 °C is not enough to complete the pore emptying by the partial elimination of organics revealed by TG (Fig. 1). Usually, the pores emptying process leads to shrinkage, and increase of apparent density due to increase of particles packing under effect of capillary pressure.[9] This scenario corresponds reasonably to the nanostructural evolution found for all films fired upon 300 °C.

It is important to recognize also that the addition of Acac ligand favours the formation of nanocrystalline anatase, but the crystallite size of dried powders is practically independent on the [Acac]/[Ti] ratio. On the other hand, the crystallite growth under firing is mainly dependent on [Acac]/[Ti]. For films with [Acac]/[Ti] = 1 and 2 the crystallite growth is fully inhibited upon firing at 400 °C, while a considerable growth is observed for the other samples treated at the same temperature. These features suggest an opposite role of Acac: (i) the maintenance of the initial crystallite size is favoured by the increase of Acac ligand anchored at the particles surface; (ii) the heat release during the combustion of organics increases with the Acac content (Fig. 1), favoring both the crystallite growth and the densification of films. This explains also the high values of apparent density, close to the anatase single crystal one (3.89 g cm^{-3}), found after firing at 400 or 500 °C (Table 1).

4. Conclusions

Anatase nanocrystalline thin films deposited by dip coating from a suspension of surface modified nanoparticles using *para*-toluene–sulfonic acid and acetylacetone exhibit both a fine intra-agglomerate and a coarse inter-agglomerate porosity. The maintenance of the initial crystallite size (9 Å) after firing upon 400 °C is achieved by the presence of acetylacetone ligand anchored at the surface of primary particle.

The heat release during the combustion of organics derivatives favors the crystallite growth and the densification of films at low sintering temperature ($\leq$500 °C). Thus, this finding allows us to use the sol–gel process to prepare dense films at the temperature range compatible with the requirements of classical glass coating technology.

Acknowledgements

The authors thank the collaboration of LNLS staff during SAXS measurements and the financial support from CNPq and FAPESP.

References

1. Zhu, Y. C. and Ding, C. X., Characterization of plasma sprayed nanotitania coatings by impedance spectroscopy. *J. Eur. Ceram. Soc.*, 2000, **20**, 127–132.
2. Traversa, E., Di Vona, M. L., Licoccia, S., Sacerdoti, M., Carota, M. M., Gallan, M. *et al.*, Sol–gel nanosized semiconducting titânia-based powders for thick films gas sensors. *J. Sol–gel Sci. Tech.*, 2000, **19**, 193–196.
3. Gräetzl, M., Sol–gel processed TiO_2 films for photovoltaic applications. *J. Sol–gel Sci. Tech.*, 2001, **22**, 7–13.
4. Hashizume, M. and Kunitake, T., Preparation of self-supporting ultra-thin films of titania by spin coating. *Langmuir*, 2003, **19**, 10172–10178.
5. Koelsch, M., Cassaignon, S., Guillemoles, J. F. and Jolivet, J. P., Comparison of optical and electrochemical properties of anatase and brookite TiO_2 synthesized by sol–gel method. *Thin Solid Films*, 2002, **403 and 404**, 312–319.

6. Scolan, E. and Sanchez, C., Synthesis and characterization of surface-protected nanocrystalline titania particles. *Chem. Mater.*, 1998, **10**, 3217–3223.
7. Hoebbell, D., Reinert, T., Schmidt, H. and Arpac, E., On the hydrolytic stability of organic ligands in Al-, Ti- and Zr-alkoxide complexes. *J. Sol–gel Sci. Tech.*, 1997, **10**, 115–126.
8. Nèvot, L. and Croce, P., Characterization of surfaces by grazing X-ray reflection—application to study of polishing of some silicate-glasses. *Rev. Phys. Appl.*, 1980, **15**, 761–769.
9. Rizzato, A. P., Broussous, L., Santilli, C. V., Pulcinelli, S. H. and Craievich, A. F., Structure of SnO_2 alcosols and films prepared by sol–gel dip coating. *J. Non-Cryst. Solids*, 2001, **284**, 61–67.
10. Beaucage, G., Ulibarri, T. A., Black, E. P. and Schaefer, D. W., Multiple size scale structures in silica-siloxane composites studied by small-angle scattering. In *American Chemical Society Symposia Proceedings, vol. 585*, ed. J. E. Mark, C. Y. C. Lee and P. A. Bianconi. American Chemical Society, Washington, 1995, pp. 97–111.